Food Hydrocolloids 125 (2022) 107376

Contents lists available at ScienceDirect

Food Hydrocolloids

journal homepage: www.elsevier.com/locate/foodhyd

Acid-induced gels from soy and whey protein thermally-induced mixed aggregates: Rheology and microstructure

Wenjie Xia [a], Linfeng Zhu [a], Roy J.B.M. Delahaije [a], Zhe Cheng [b], Xilong Zhou [a], Leonard M. C. Sagis [a,*]

[a] Physics and Physical Chemistry of Foods, Department of Agrotechnology and Food Sciences, Wageningen University & Research, Bornse Weilanden 9, 6708WG, Wageningen, the Netherlands

[b] Food Quality and Design, Department of Agrotechnology and Food Sciences, Wageningen University & Research, Bornse Weilanden 9, 6708WG, Wageningen, the Netherlands

ARTICLE INFO

Keywords:
Protein mixtures
Glucono-δ-lactone (GDL)
Cold-set gels
Small amplitude oscillatory shear (SAOS)
Large amplitude oscillatory shear (LAOS)
Lissajous plots

ABSTRACT

In this study, we explored how substituting whey protein isolate (WPI) with soy protein isolate (SPI) affects the linear and non-linear rheological behavior of acid-induced gels, and their microstructures. Commercial SPI and WPI dispersions (pH 7.0, 3.0 mS/cm) were preheated (95 °C, 30 min) at different protein concentrations (2%, 4%, 6%, and 8% w/w) and SPI: WPI ratios (0: 4, 1: 3, 2: 2, 3: 1 and 4: 0). The resultant thermally-induced aggregates were characterized before gelation was induced by glucono-δ-lactone (GDL). Small and large amplitude oscillatory shear (SAOS and LAOS) tests showed that replacing WPI with SPI decreased the strength (lower G′) and stretchability (lower γ_c) of acid-induced gels in the linear viscoelastic (LVE) regime. Gels containing SPI behaved more similar to pure SPI gels in the non-linear viscoelastic (NLVE) regime: displaying a relatively elastic response at large strain and a gradual transition to plastic behavior. The changes in rheological properties were explained by the differences in the gel microstructures, via fractal scaling theory, multiphoton laser scanning microscopy (MLSM) and scanning electron microscopy (SEM). WPI gels formed denser and homogenous gel networks with very strong inter-floc links, while hybrid gels and pure SPI gels formed coarser and more porous networks with intermediate inter-floc links. The constituent flocs in the latter were larger, with rougher, more elongated and branched structures. The present results provide useful information for future attempts to replace WPI with SPI in food products based on acid-induced gelation.

1. Introduction

The demand for food protein has grown dramatically due to the global population increase. This demand cannot be met by simply increasing the supply of traditional animal-based proteins such as meat and dairy protein, considering their high ecological footprint and production cost compared to plant-based proteins (Day, 2013). Dairy proteins, i.e. caseins and whey proteins, have been widely used as gelling agents in texturized foods such as cheese, yoghurt, and pudding. If they can be partially or completely substituted by plant proteins in these gel-based products, the new formulations will not only be more sustainable, but also bring more choices and nutritional values to the consumer (Day, 2013; Wu et al., 2020).

Gelation of food proteins is a complex process that involves several reactions such as denaturation, dissociation-association, aggregation and gelation (Hermansson, 1986). This process is usually induced by heat treatment, and the properties of heat-set gels have been extensively studied (Nicolai & Chassenieux, 2019; Xia, Siu, & Sagis, 2021). On the other hand, protein gelation can also be induced by acidulating agents, such as glucono-δ-lactone (GDL). Acid-induced gelation occurs in the production of many food products, such as yoghurt and silken tofu. In contrast to heat-induced gelation where the denaturation, aggregation and gelation are intertwined and occur simultaneously, acid-induced gelation often consists of two separate steps: Firstly, protein solutions are preheated at neutral pH and a relatively low concentration to induce protein denaturation and aggregation. Secondly, acidulating agents are used to decrease the pH of the protein aggregate dispersions. This reduces the net charge of the proteins and hence the electrostatic repulsion between them, leading to further aggregation and gel formation (Alting, Hamer, De Kruif, & Visschers, 2000; Bryant & Julian McClements,

* Corresponding author.
E-mail address: leonard.sagis@wur.nl (L.M.C. Sagis).

https://doi.org/10.1016/j.foodhyd.2021.107376
Received 9 September 2021; Received in revised form 15 November 2021; Accepted 16 November 2021
Available online 19 November 2021

1998). Since the gelation step can be performed at ambient temperature, acid-induced gels are also known as cold-set gels. They can be used to encapsulate heat-sensitive or volatile compounds in the food, pharmaceutical and cosmetic sectors (Abaee, Mohammadian, & Jafari, 2017).

The properties of acid-induced gels can be influenced by the conditions of preheating and gelation processes (e.g. temperature, time, pH, and ionic strength) as well as the concentration and composition of proteins (Britten & Giroux, 2001; de Faria, Minim, & Minim, 2013; Kharlamova, Chassenieux, & Nicolai, 2018; Schmitt, Silva, Amagliani, Chassenieux, & Nicolai, 2019). For acid-induced hybrid gels formed by mixed dairy and plant proteins, the properties can be expected to vary significantly with composition, since proteins from different origins normally possess different structures, thermal transition temperatures, isoelectric points, and gelling properties (Wu et al., 2020). For the preheating step these hetero-proteins can be heated separately or simultaneously, leading to "a mixture of aggregates" or "mixed aggregates", which would also result in different gel properties (Chihi, Sok, & Saurel, 2018). Up-to-now, studies have been reported on acid-induced hybrid gels formed by pea and whey proteins (Chihi et al., 2018; Schmitt et al., 2019), pea protein and casein micelles (Mession, Roustel, & Saurel, 2017), soy protein and sodium caseinate (Martin, De Los Reyes Jiménez, & Pouvreau, 2016), and soy protein and casein micelles (Roesch & Corredig, 2006). Information on acid-induced gelation of whey and soy protein mixtures is still limited, although it is of both fundamental and applied interest.

The practical application of a gel system calls for a comprehensive understanding of its rheological properties. To characterize these properties, dynamic oscillatory shear tests are commonly performed, during which a gel material is subjected to a sinusoidal deformation, and the resulting mechanical response is measured (Hyun et al., 2011). Based on the amplitude of deformation, dynamic oscillatory shear tests can be divided into two categories: small amplitude oscillatory shear (SAOS) and large amplitude oscillatory shear (LAOS) tests. In SAOS tests, the strain amplitudes are too small to disrupt the gel microstructure, and the mechanical response of gels is in the linear viscoelastic (LVE) regime, i.e. the viscoelastic moduli (G′ and G″) are independent of the applied stress or strain (Precha-Atsawanan, Uttapap, & Sagis, 2018). In LAOS tests, on the other hand, the strain amplitude is increased to a level where the gel microstructure is affected, and the rheological properties in the non-linear viscoelastic (NLVE) regime can be revealed (Xia et al., 2021).

As mentioned in a recent review article by Joyner (2021), despite LAOS tests are still far from the mainstream of the food science field, it is a valuable tool for investigating the interplay of food microstructures, textures, processing properties, and sensory properties, since food products inevitably undergo remarkably large deformation during production (e.g. mixing and pumping) and digestion processes (e.g. chewing and swallowing). The research group of Melito (2011, 2012, 2013a, 2013b) has applied LAOS tests on whey protein isolate/κ-carrageenan gels and different kinds of commercial cheeses, which demonstrated that the sensory and oral processing characteristics of food gels can be well correlated to their rheological properties in the NLVE regime. Bi, Li, Wang, and Adhikari (2017, 2018) found the acid-induced hybrid gels of soy protein and locust bean gum/κ-Carrageenan displayed intercycle strain softening behavior in the NLVE regime. This behavior was also found when the fermentation-induced pea protein gels were subjected to LAOS tests, but these gels displayed intracycle strain stiffening behavior when the amplitude was between 1.6% and 160%, and intracycle shear thinning behavior when the amplitude exceeded 160% (Klost, Brzeski, & Drusch, 2020; Klost, Giménez-Ribes, & Drusch, 2020). LAOS tests have also been applied on gelatin gels (Goudoulas & Germann, 2017; Yang et al., 2016), waxy rice starch gels (Precha-Atsawanan et al., 2018), pectin-Ca gels (John, Ray, Aswal, Deshpande, & Varughese, 2019), and concentrated protein gels (Schreuders et al., 2021), to provide more comprehensive information on the linear and non-linear rheological behaviors of these food gel matrices.

Dairy proteins can be used to control the structure and texture of food products. Whey protein, for example, has been known to significantly affect the rheological properties of foods when processed under shear or different physicochemical environments (Mccann, Guyon, Fischer, & Day, 2018). Heating milk before acidification could cause denaturation and induce attractive interactions between whey proteins, which conferred higher elastic moduli (G′) to the milk gels (Roesch, Juneja, Monagle, & Corredig, 2004). Adding whey protein to milk before this thermal treatment also enhanced the gel firmness and reduced syneresis (Anema, 2018). Soy protein, a plant-based protein that has been widely consumed in Asia, is also known for its contribution to food texture, as well as its high nutritional value and availability (Nagano, Mori, & Nishinari, 1994). In our recent work, we applied both SAOS and LAOS tests on soy protein heat-set gels and characterized their rheological behavior in both the LVE and NLVE regimes (Xia et al., 2021). Nevertheless, it remains unclear that how mixing soy protein with whey protein affects the "rheological fingerprint" of acid-induced gel matrices, especially in the NLVE regime.

In this study, we investigated the rheological properties and microstructure of acid (GDL)-induced gels formed by blends of commercial whey protein isolate (WPI) and soy protein isolate (SPI). Before acidification, WPI and SPI were preheated together at different ratios and concentrations, and thus mixed aggregates were formed. The properties of these thermally-induced aggregates were characterized by dynamic light scattering (DLS), size exclusion chromatography (SEC), surface hydrophobicity (H_0), and intrinsic fluorescence spectroscopy. Subsequently, these aggregates were used to form acid-induced gels, of which the linear and non-linear viscoelastic properties were studied by SAOS and LAOS tests, and the water holding capacity (WHC) and gel solubility were also determined. We applied Lissajous-Bowditch plots to interpret the LAOS data, and used fractal scaling theory to link the rheological behaviors to the gel microstructure (characterized by multiphoton laser scanning microscopy (MLSM) and scanning electron microscopy (SEM)). This study will benefit the application of soy protein in traditional dairy products based on acid-induced gelation.

2. Materials and methods

2.1. Materials

Commercial SPI (Unisol NRG IP Non-GMO) was provided by Barentz International B.V. (Hoofddorp, North Holland, the Netherlands). Commercial WPI (BiPRO® 9500) was bought from AGROPUR Dairy Co. (Longueuil, Quebec, Canada). The protein content of SPI and WPI were 86.57 ± 0.18% ($N \times 6.25$) and 92.26 ± 0.29% ($N \times 6.38$) respectively, determined by Dumas combustion method with a FlashEA 1112 N/Protein Analyzer (Thermo Fisher Scientific, Waltham, MA, USA). Glucono-δ-lactone (GDL) (Art. No. G4750) and other chemical reagents were ordered from Sigma-Aldrich Co., (St. Louis, MO, USA). Deionized distilled water (DDW) used in the study was purified by a PURELAB Ultra apparatus (ELGA LabWater Co., High Wycombe, UK). Unless mentioned otherwise, all experiments were performed in thermostatic laboratories (20 ± 1 °C).

2.2. Sol-gel phase diagram

Commercial SPI and WPI powders were dissolved in DDW at different protein concentrations and stirred overnight to ensure complete hydration. SPI and WPI dispersions of the same concentration were mixed at different ratios and heated simultaneously at 95 °C, pH 7.0 for 30 min. Subsequently, a sol-gel phase diagram was established for these heated protein samples according to the method of Chihi et al. (2018). To determine the critical thermal gelation concentrations (C_{gth}), the samples after heating (5 mL) were immediately poured into 15 ml CELLSTAR® tubes with screw caps (Art. No. 188271, Greiner Bio-one B. V., the Netherlands) and vertically stored at 4 °C for 24 h. After this, the

samples that were not flowing under tube inversion were considered as heat-set gels, and the minimum concentration to form these gels was considered as C_{gth}. To determine the critical acid gelation concentration (C_{ga}), samples (5 ml) with protein concentrations below C_{gth} were transferred into 15 ml CELLSTAR® tubes after heating. When the samples were cooled to room temperature, appropriate amounts of GDL powder (20% of total protein content) were added (Eissa & Khan, 2005). The resulting samples were incubated at 40 °C for 3 h and then stored at 4 °C for 24 h. Those not flowing under tube inversion were considered as acid-induced gels, and the minimum concentration to form gels was considered as C_{ga}.

2.3. Characterization of SPI and WPI thermally-induced aggregates

The effects of SPI: WPI ratio on the properties of thermally-induced aggregates were studied using samples with a 4% w/w protein concentration. SPI and WPI dispersions (4% w/w) were prepared and mixed at five ratios (4:0, 3:1, 2:2, 1:3, 0:4). The pH and conductivity of these dispersions were standardized to pH 7.0 and 3.0 mS/cm (~55 mM ionic strength) by adding 2 mol/L NaOH or HCl solutions or NaCl powder. Subsequently, each dispersion was divided into two parts for the following tests. One part was heated at 95 °C, pH 7.0 for 30 min while the other one was not heated and served as a control.

2.3.1. Dynamic light scattering (DLS)

The particle size and zeta-potential of samples were measured by DLS using a Zetasizer Nano ZS (Malvern Instruments, Worcestershire, UK). Sample dispersions were diluted to 0.3% w/w protein concentration and injected into folded capillary zeta cells (DTS1070, Malvern). The refractive and absorption indices of the particles were set at 1.450 and 0.001 respectively, while the refractive index of the dispersant (DDW) was 1.330.

2.3.2. Size exclusion chromatography (SEC)

Sample dispersions were centrifuged at 15,000 g for 10 min before SEC analysis. The supernatants (50 μL) were injected on an ÄKTA pure 25 system (Cytiva, Marlborough, MA, USA) equipped with Superose® 6 10/300 GL column, and eluted with sodium phosphate buffer (30 mM, pH 7.0) containing 50 mM NaCl at a flow rate of 0.5 mL/min. The elution was monitored using UV absorbance at 214 nm. The column was calibrated with a series of biomacromolecules with molecular weights ranging from 29 to 2000 kDa (MWGF-1000, Sigma-Aldrich, USA). The calibration curve of these standard samples is provided in the supplementary material (Fig. S1).

2.3.3. Surface hydrophobicity (H_0)

The H_0 of samples was determined using 8-anilino-1-napthalenesulfonic acid ammonium salt (ANSA) as a fluorescent probe. Each sample dispersion was diluted with DDW to obtain a sequence of protein concentrations (0.0025%, 0.005%, 0.01%, 0.02% w/w), and were added into acrylic cuvettes (Sarstedt Inc, Nümbrecht, Germany) together with 40 μL of ANSA reagent (8 mM). After 1-h reaction in the dark, the fluorescence intensity (FI) of these samples was measured by a luminescence spectrometer LS50B (PerkinElmer, Waltham, MA, USA) at an excitation wavelength (λ_{Ex}) of 390 nm and emission wavelength (λ_{Em}) of 470 nm. The slope of the entirely linear curve of FI vs. protein concentration was used as the indicator of H_0.

2.3.4. Intrinsic fluorescence spectra

Intrinsic fluorescence spectra of samples were measured according to the method of Wan, Li, and Guo (2021). The sample dispersions were adjusted to 0.02% w/w and their intrinsic fluorescence spectra were determined using a PerkinElmer (LS50B) luminescence spectrometer. A volume of 3 mL of each sample was slowly added into a 10 mm path length quartz cuvette (Hellma GmbH). The λ_{Ex} was set at 295 nm, and the λ_{Em} was recorded from 300 to 500 nm. Both the excitation and emission slit were 5 nm.

2.3.5. Protein solubility

The protein solubility of samples was evaluated by measuring the protein content in the supernatant after centrifugation. Sample dispersions (20 ml) were added in 50 ml centrifuge tubes (Sarstedt Inc) and then centrifuged at 15,000 g for 10 min. The protein concentration of supernatants was measured by the Dumas combustion method. Protein solubility of different samples was expressed as below:

$$Protein\ solubility\ (\%) = \frac{Protein\ content\ supernatant}{Total\ protein\ content} \times 100\%$$

2.4. Rheology of acid-induced gelation

The process of acid-induced gelation and the rheological properties of the resultant gels were studied using an MCR 302 rheometer (Anton Paar, Graz, Austria) with a titanium sandblasted concentric cylinder geometry (CC17). SPI and WPI dispersions at different protein concentrations (2%, 4%, 6% and 8% w/w) were prepared, and then mixed at different ratios (4:0, 3:1, 2:2, 1:3, 0:4). Each protein mixture was heated at 95 °C, for 30 min. After this, the preheated samples were cooled to room temperature and mixed with appropriate amounts of GDL (20% of total protein content). Immediately, a volume of 4.7 ml protein sample was gently injected into the CC17 cup that was preheated at 40 °C. The CC17 cup was covered with a solvent trap to prevent sample evaporation. In the following rheological tests, the temperature was controlled by a Peltier element and a water circulation system.

2.4.1. Small amplitude oscillatory shear (SAOS) tests

SAOS tests were performed at a fixed amplitude of 0.1% and a frequency of 0.1 Hz, which were within the linear viscoelastic (LVE) regime. First, oscillations were applied at 40 °C for 3 h, and then the temperature was decreased from 40 °C to 4 °C at a rate of 1 °C/min. After this, the formed gels were allowed to rest at 4 °C for 5 min, before performing a frequency-sweep test from 0.1 to 10 Hz (4 °C), at an amplitude of 0.1%. The storage modulus (G′), loss modulus (G″), and loss tangent (tan δ) were recorded throughout the SAOS tests. The change of G′ and G″ as a function of frequency was fitted with a Power-law model.

2.4.2. Large amplitude oscillatory shear (LAOS) tests

After the frequency-sweep test in Section 2.4.1, the gels were subjected to a LAOS amplitude-sweep test to investigate their viscoelastic behavior in the non-linear viscoelastic (NLVE) regime. The strain amplitude (γ_0) was increased from 0.1% to 1000% in a ramp logarithmic mode at a fixed frequency (0.1 Hz) and temperature (4 °C). The G′ and G″ were monitored as a function of intercycle strain (γ_0) while the shear stress (σ) was monitored as a function of intracycle strain (γ) and strain rate ($\dot{\gamma}$). Lissajous-Bowditch plots (also called Lissajous plots) were constructed to analyze the NLVE properties of these gels. In these plots, the oscillating stress signal σ(t) is plotted directly against the oscillating strain γ(t) or strain rate $\dot{\gamma}$ (t), leading to elastic or viscous Lissajous plots, respectively. In the elastic curves we also plotted the elastic contribution to the total stress, and likewise, we plotted the viscous contribution to the total stress in the viscous Lissajous plots. As extensively discussed by Ewoldt, Hosoi, and McKinley (2008), the analysis framework using Lissajous plots can effectively reveal the different non-linear rheological responses of materials.

2.5. Acidification kinetics

The effects of SPI: WPI ratio on the acidification kinetic during GDL-induced gelation were studied using samples with a 4% w/w protein concentration. In brief, SPI and WPI dispersions were prepared and mixed at five ratios (4:0, 3:1, 2:2, 1:3, 0:4) as in Section 2.4. Then, the

dispersions were heated at 95 °C, pH 7.0 for 30 min and cooled to room temperature. After mixing with GDL powder (0.8% w/w), the dispersions were incubated in a water bath at 40 °C for 3 h, during which their pH were recorded every 10 min by a pH-meter (SCHOTT Instruments, Mainz, Germany).

2.6. Water holding capacity (WHC)

The WHC of acid-induced gels was determined based on the method of Kocher and Foegeding (1993). A microcentrifuge filtration unit (i.e. a 2 ml Eppendorf tube with a spin tube inside). was used (Axygen Biosciences, Inc., Union City, USA). Filter paper was used to reduce grid size. Protein gels (4% w/w, 0.5 mL) were prepared in the same manner as in the rheology test (Section 2.4) and centrifuged at 500 g for 10 min (Z306 centrifuge, HERMLE Labortechnik, Wehingen, Germany). The water expelled from the gel was collected in the outer Eppendorf tube. The WHC was defined as the percentage of the water that remaining in the gel after centrifugation:

$$WHC = (W_T - W_E)/ W_T \times 100\ [\%]$$

where W_T is the total amount of water before gelation (g), and W_E is the amount of water expelled from the gel (g).

2.7. Gel solubility

The solubility of acid-induced gels was determined according to previous studies (Chu, Yang, Li, Lin, & Zheng, 2019; Gu, Campbell, & Euston, 2009). Protein gels (4% w/w, 10 ml) were formed in 50 ml centrifuge tubes (Sarstedt Inc) before mixing with 10 ml of each of the following solvents: (S_A) DDW; (S_B) 0.086 M Tris, 0.09 M glycine, 4 mM Na_2EDTA buffer (pH 8.0); (S_C) S_B containing 1% SDS and 8 M urea; (S_D) S_C containing 5% 2-mercaptoethanol. After this, the tubes were rotated by a rotator (Labinco BV, Breda, The Netherlands) for 48 h and then centrifuged at 15,000 g for 10 min (Z383K centrifuge, HERMLE Labortechnik GmbH, Wehingen, Germany). Soluble protein content in the supernatant was determined using a Pierce™ detergent compatible Bradford assay kit (No. 23246, Thermo Fisher Scientific). The gel solubility in different solvents was expressed as below:

$$Gel\ solubility\ (\%) = \frac{Protein\ content\ supernatant}{Total\ protein\ content} \times 100\%$$

Tris-glycine buffers can screen electrostatic interactions, SDS and urea are known to disrupt hydrophobic interactions and hydrogen bonds, and 2-mercaptoethanol is a bond-breaking agent for disulfide bonds. The differences in gel solubility in different solvents (i.e. S_B- S_A, S_C- S_B, and S_D- S_C) were used to indicate the relative importance of different interactions for maintaining the gel structures.

2.8. Microscopy of the acid-induced gels

2.8.1. Multiphoton laser scanning microscopy (MLSM)

Alexa Fluor® 350 (λ_{Ex}: 800 nm, λ_{Em}: 570–630 nm) and Cy5® (λ_{Ex}: 840 nm, λ_{Em}: 650–700 nm) were dissolved in dimethyl sulfoxide at 1 mg/mL, and then used to stain WPI and SPI dispersion (4% w/w), respectively. Then, these two dispersions were mixed at different ratios before mixing with GDL (0.8% w/w). Immediately, 120 μL of each mixture was transferred to hermetically sealed flat cuvettes (Gene Frame® 125 μL, Thermo Fisher Scientific, Waltham, MA, USA) that were glued onto microscopy slides in advance. After covering with coverslips, these microscopy slides were mounted on a Peltier system (LTS120, LINKAM. Co., UK) to allow acid-induced gels to form in the same manner as in the rheology tests (40 °C for 3 h and cooled to 4 °C at the rate of 1 °C/min). The gel samples were visualized by a Leica SP8Dive multiphoton excitation microscope (Leica, Germany), using a HC FLUOTAR L 25 × /0.95 W VISIR objective.

2.8.2. Scanning electron microscopy (SEM)

Acid-induced gels (4% w/w, 5 mL) were prepared in 10 ml disposable thermotolerant syringes (Terumo Corporation, Tokyo, Japan) with the tip sealed by a syringe screw cap (Combi™ plug, Becton Dickinson, Franklin Lakes, NJ, USA). For SEM imaging, the gels formed in the syringes were cut into small cubes (~5 × 5 × 5 mm) and fixed in 2.5% glutaraldehyde for at least 8 h. After the crosslinking, the samples were rinsed to remove the excess of glutaraldehyde and were dehydrated using a series of ethanol (30%, 50%, 70%, 80%, 90%, 100%) solutions before critical point drying (CPD 300, Leica, Vienna, Austria). Subsequently, the samples were fractured and attached to SEM sample holders using Carbon Conductive Cement (Leit-C, Neubauer Chemicalien, Germany). After sputter coating with a 12 nm layer of tungsten (SCD 500, Leica, Vienna, Austria) the fractured surfaces were analyzed with SE detection at 2 kV in a field emission scanning electron microscope (Magellan 400, FEI, Eindhoven, the Netherlands).

2.9. Statistical analysis

All experiments were performed in duplicate at least. The statistical analysis of data was conducted by SPSS 25.0 (IBM SPSS Inc. Chicago, IL, USA). One-way ANOVA (one-way analysis of variance) with the Duncan post-Hoc test ($p < 0.05$) were used to evaluate the statistical significance of differences among means. Lissajous plots were made by MATLAB R2018b (MathWorks Inc., MA, USA) while other figures were made by Origin 2018 (Origin Lab Corporation, MA, USA).

3. Results and discussion

3.1. Sol-gel phase diagram

To investigate acid-induced gelation, it is necessary to avoid forming heat-set gels directly after the preheating step (95 °C, pH 7.0 for 30 min). A sol-gel phase diagram (Fig. 1) was established for SPI and WPI mixtures, using a series of samples covering different protein concentrations and SPI: WPI ratios. The red line in the phase diagram represents the critical thermal gelation concentration (C_{gth}), while the blue line represents the critical acid gelation concentration (C_{ga}). As shown in Fig. 1, pure SPI and WPI directly formed heat-set gels when their concentration is above 8% w/w and 10% w/w respectively, which are comparable to the C_{gth} found in previous studies (Campbell, Gu, Dewar, & Euston, 2009; Nguyen, Chassenieux, Nicolai, & Schmitt, 2017). For SPI and WPI mixtures, the C_{gth} gradually decreased from 10% to 7.5% w/w with an increasing SPI: WPI ratio, indicating the thermal gelling ability of mixtures increased as more soy protein was involved. The C_{ga} for preheated

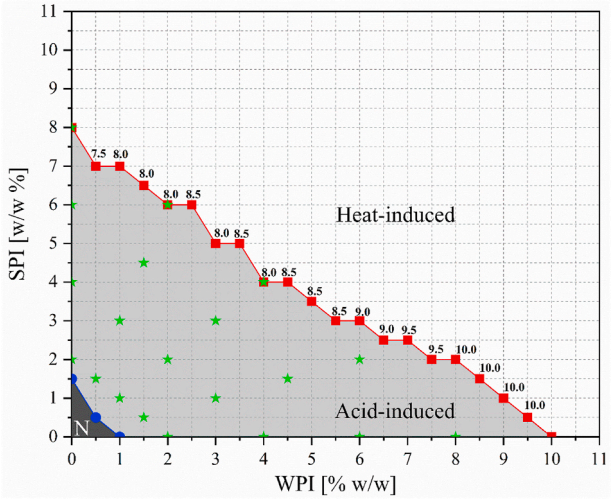

Fig. 1. Sol-gel phase diagram for SPI and WPI mixtures.

SPI and WPI were 1.5% and 1.0% w/w, respectively, and the C_{ga} for the preheated mixtures are in between. This shows that after the preheating step, GDL-induced gels can be formed by commercial SPI and WPI at very low concentrations compared to heat-set gels. Based on this phase diagram, four protein concentrations (2% w/w, 4% w/w, 6% w/w, and 8% w/w), and five SPI: WPI ratios (0:4, 1:3, 2:2, 3:1, and 4:0) were selected, to investigate acid-induced gelation of SPI and WPI mixtures.

3.2. Characteristics of thermally-induced aggregates

In the preheating step of this study (95 °C, pH 7.0 for 30 min), the mixtures of SPI and WPI formed thermally-induced aggregates, and we will first present an overview of the physical and conformational properties of these mixed aggregates before discussing the rheological and microstructural properties of the acid-induced gels formed by them.

Fig. 2A shows that the particle size distribution (PSD) (number based) of all samples moved towards larger sizes after preheating, proving the formation of protein aggregates. For instance, the peak in the PSD of pure WPI shifted from ~2 nm to ~20 nm after heating, which is comparable to results reported previously (Zhou, Sala, & Sagis, 2020). Both before and after the preheating, the PSD of mixtures shifted towards a larger size range when the proportion of SPI increased. Pure WPI and mixtures formed thermally-induced aggregates with a size between 10 and 100 nm, while pure SPI showed the existence of some large macroaggregates (>100 nm). The PSD result was obtained based on the whole protein sample, and we further applied size exclusion chromatography (SEC) to provide information on the soluble proteins and protein aggregates in the sample. As shown in Fig. 2B, the supernatants of unheated samples all displayed a unimodal SEC profile with one peak located in between 17.8 and 19.3 mL elution volume (≈18–43 kDa),

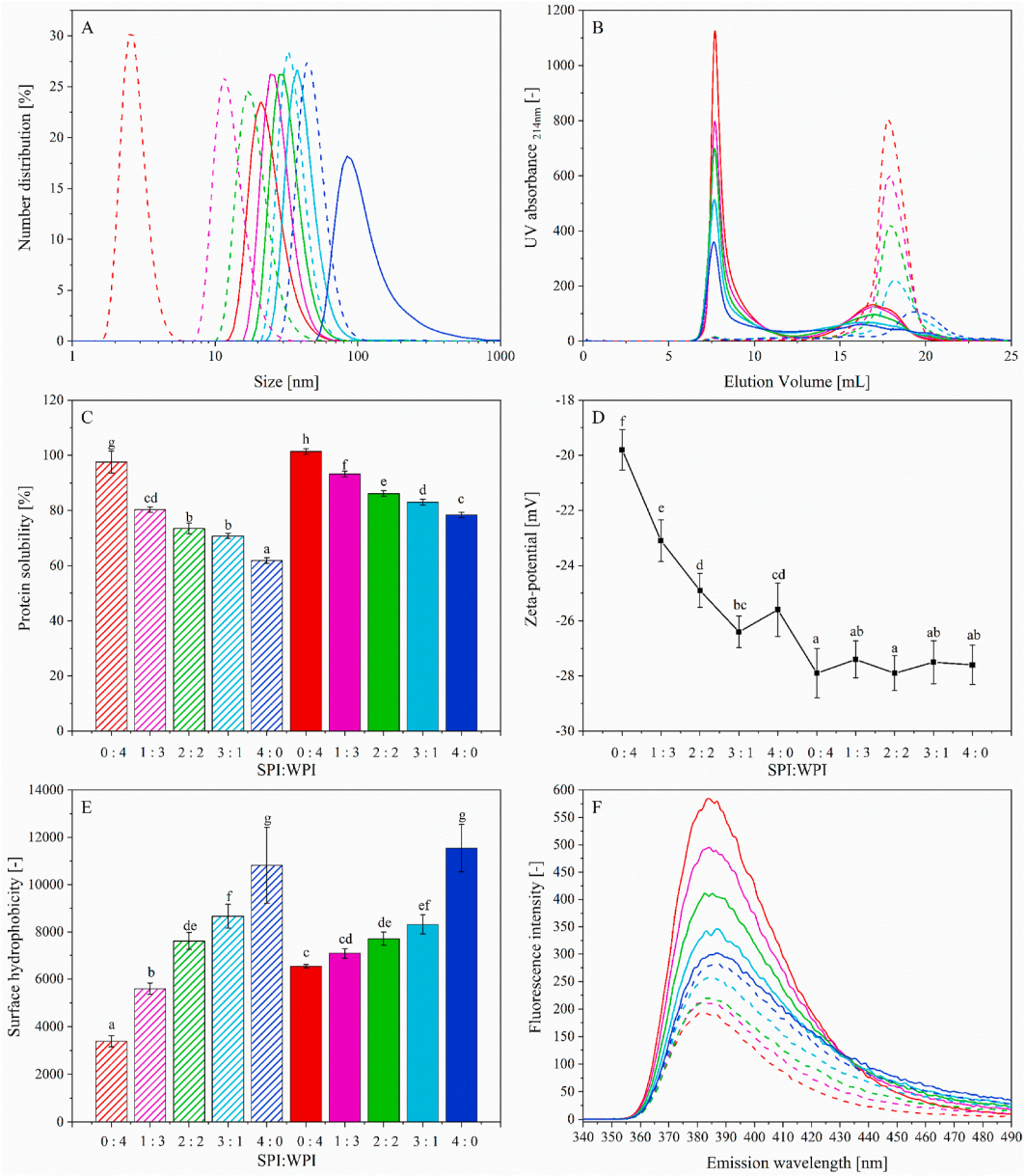

Fig. 2. Physical and conformational properties of SPI and WPI mixtures: S:W 0:4 (red), S:W 1:3 (magenta), S:W 2:2 (green), S:W 3:1 (cyan), S:W 4:0 (dark blue). Particle size distribution (A), size exclusion chromatography of supernatant (B) and protein solubility (C), zeta potential (D), surface hydrophobicity (E), and intrinsic fluorescence spectra (F). Dashed line/bar represents non-heated mixtures (control group), while solid line/bar represents samples after preheating. Different small letters (in the same subplot) indicates that the results of different samples are significantly different ($p < 0.05$) according to ANOVA and Duncan post-Hoc test. (For interpretation of the references to color in this figure legend, the reader is referred to the Web version of this article.)

which can be attributed to protein monomers and subunits (Nishinari, Fang, Guo, & Phillips, 2014; Wang & Guo, 2019). After preheating, the SEC profiles of all supernatants changed to a bimodal distribution, with a new peak appearing at around 7.6 mL elution volume (≈17 × 10^3 kDa), representing the formation of soluble protein aggregates. As the SPI: WPI ratio increased, the location of this new peak did not change while its intensity decreased significantly, suggesting the size of soluble aggregates were similar but their amount decreased with increasing SPI proportion. Combined with the PSD results, it can be deduced that replacing WPI with SPI led to an increased formation of insoluble aggregates and a decrease in the fraction of smaller soluble aggregates. This analysis is also supported by protein solubility results (Fig. 2C) which displayed a linear relationship with the enclosed area of SEC peaks (Fig. S2). The preheating step increased the protein solubility of all samples significantly. After heating, the solubility showed a decreasing trend as more SPI was involved, due to a lower proportion of soluble aggregates.

Fig. 2D shows that the zeta-potential of all samples was negative at pH 7.0, since this pH was above the isoelectric point of soy and whey proteins. For unheated samples, the zeta-potential decreased as the proportion of SPI increased. They all decreased to a similar level (around −28mV) after heating, indicating the surface charge and electrostatic interactions of thermally-induced aggregates were similar and not affected by SPI: WPI ratios. Ryan et al. (2012) reported that heating WPI for 10 min at 90 °C and pH 7.0 generated soluble WPI aggregates that had a more negative surface charge than unheated WPI. Wan et al. (2021) recently found that the change in zeta-potential of SPI upon formation of aggregates was relatively small and dependent on the protein concentration during heating. Fig. 2E shows that the surface hydrophobicity (H_0) of unheated samples gradually increased with the proportion of SPI. This could be attributed to the harsh industrial processing of commercial SPI which resulted in a large extent of protein denaturation and unfolding, exposing more hydrophobic groups to the protein surface (Spotti et al., 2019). The preheating step also induced the denaturation of commercial WPI, leading to higher H_0, but did not increase the H_0 of samples containing a high proportion of SPI. Consistently, the intrinsic fluorescence spectra (Fig. 2F) of unheated samples showed a gradual red shift (increased λ_{max}) as the proportion of SPI increased, indicating that Tryptophan residues were exposed to a more polar/hydrophilic environment due to unfolded soy protein structures (Wan et al., 2021). After the preheating, although the λ_{max} of all samples further increased, the λ_{max} was still higher for the samples with more SPI, indicating that their thermally-induced aggregates consisted of proteins that were more unfolded.

3.3. Acidification kinetics

During the isothermal incubation (40 °C), the slow hydrolysis of GDL into gluconic acid releases protons, which subsequently reduce electrostatic repulsion between aggregates by protonation of charged carboxyl groups, and induce their aggregation into a three-dimensional (3D) gel network (Chihi et al., 2018). It is known that the acidification kinetics of GDL depend on the protein: GDL ratio as well as the temperature. To determine how different SPI: WPI ratios would affect the acidification kinetics, we recorded the pH of dispersions of thermally-induced aggregates (4% w/w) formed at different SPI: WPI ratios at the same amount of GDL addition (0.8% w/w) and temperature (40 °C). As shown in Fig. 3, all samples displayed similar acidification kinetics: the decrease in pH was fastest in the beginning, then slowed down and finally leveled off. Pure WPI showed a faster acidification rate than pure SPI, as it took 100 min for WPI to reach pH 4.5 (the pKa of glutamic acid) while 180 min for SPI. Similarly, for mixed aggregates a higher SPI fraction led to a slower pH decreasing rate. This phenomenon could be attributed to the buffering ability of soy protein (Roesch et al., 2004). The acidification rate might affect the level of structural rearrangements during gelation and thus the gel properties (Nicolai, Britten, & Schmitt, 2011). For example, it has been reported that bacterial-acidification-induced WPI gels showed increased hardness when the acidification rate was faster (Alting, Van Der Meulena, Hugenholtz, & Visschers, 2004), which is in line with our subsequent rheology results.

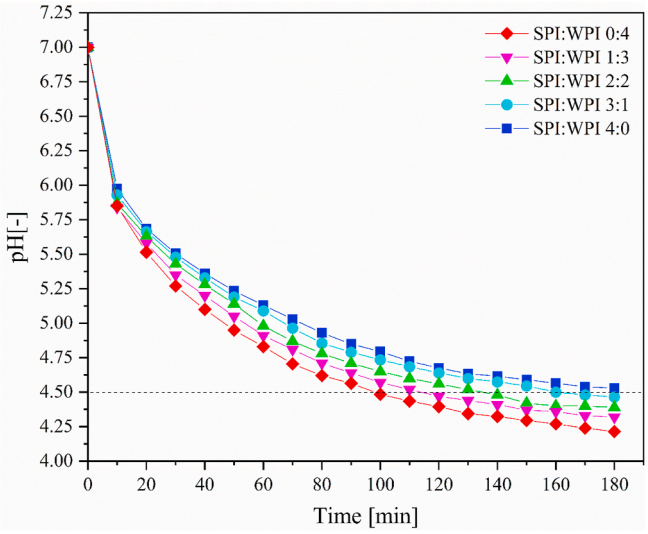

Fig. 3. Acidification kinetics (3 h) of the dispersions of thermally-induced aggregates (4% w/w).

3.4. Linear rheology

Small amplitude oscillatory shear (SAOS) tests were used to investigate the acid-induced gelation kinetics of preheated samples and characterize the linear viscoelastic (LVE) properties of the gels. Fig. 4 shows the results of 4% w/w protein samples which were used as representative samples. As shown in Fig. 4A, all samples displayed a similar GDL-induced gelation profile, regardless of composition and concentration (data not shown): after a short lag phase, the G′ and G″ started to increase rapidly, and subsequently the gelation rate slowed down, until the moduli reached a plateau. The time when G′ exceeds 1Pa is often taken as the gelling point of acid-induced gels (Wan et al., 2021). It was found that all samples started to gel within 30 min, and the gelling point was postponed when the proportion of SPI increased. As rementioned above, the zeta-potentials of preheated samples were similar while H_0 was higher with increasing proportion of SPI. This implies that the postponed gelling point is most likely due to the slower acidification rate of SPI, resulting in a longer time for the attractive interactions such as hydrophobic interactions to overcome the electrostatic repulsive force. For gels formed at the same protein concentration, replacing WPI with SPI significantly decreased the final G′ at 40 °C (Table 1), indicating a lower gel strength. Schmitt et al. (2019) concluded that the presence of plant proteins led to a lower gel strength compared to dairy proteins alone, because the different proteins appeared to form separate gel networks which did not interact with each other. This is also consistent with our microscopy results that will be shown later.

Fig. 4B shows that the G′ and G″ of acid-induced gels further increased when lowering the temperature from 40 °C to 4 °C, which suggested reinforcement or rearrangement of the gel structure during the cooling process. According to previous studies, this increase in moduli was mainly due to the formation of hydrogen bonds (Li et al., 2020; Zhao et al., 2020). Table 1 shows that the enhancement of G′ during this cooling processing ($\Delta G' = [G'(4°C) - G'(40°C)]/G'(40°C)$) varied with the protein composition of gels but not the protein concentration. Gels that contained more SPI showed higher ΔG′, indicating this strengthening effect of cooling was more significant. This indicated that hydrogen bonds might play a more important role in maintaining

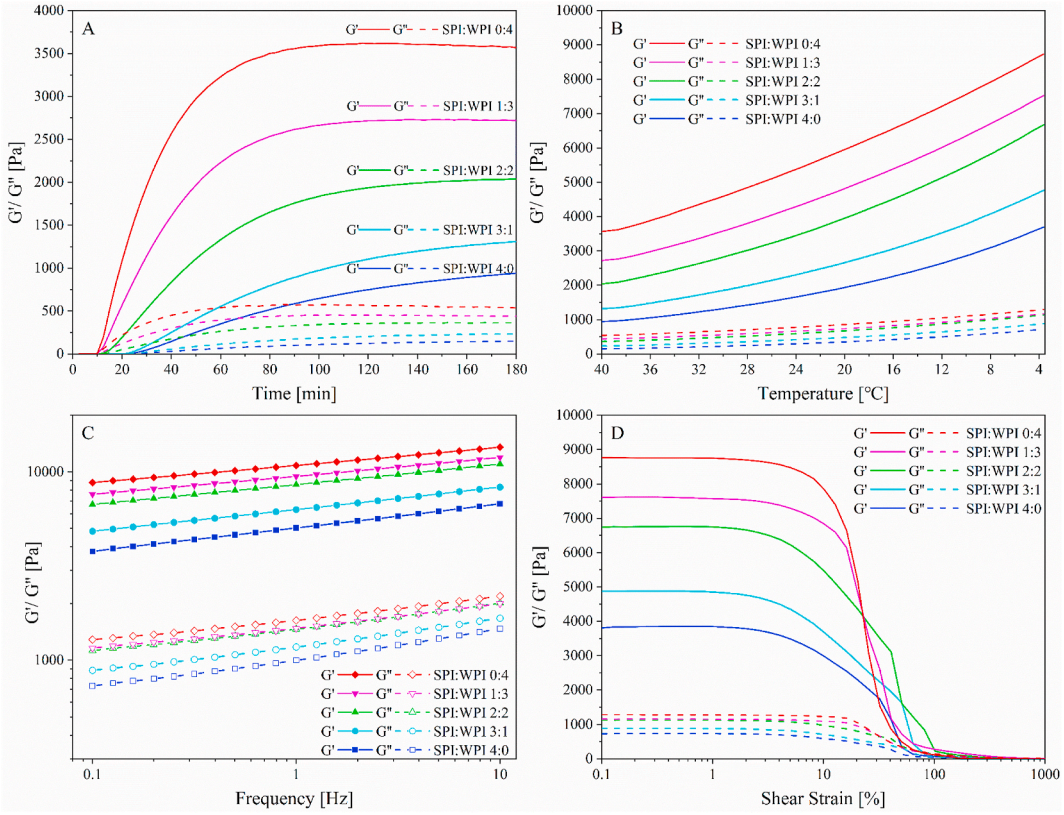

Fig. 4. Time sweep (A) and temperature sweep (B) tests of the dispersions of thermally-induced aggregates (4% w/w), and frequency sweep (C) and strain sweep (D) of the resultant gels.

Table 1
Storage modules (G′) of the acid-induced gels formed at different SPI:WPI ratios during temperature sweep test.

SPI: WPI	0: 4		1: 3		2: 2		3: 1		4: 0	
Conc.	G′ (40 °C) (10^3 Pa)	ΔG′	G’ (40 °C) (10^3 Pa)	ΔG′	G’ (40 °C) (10^3 Pa)	ΔG′	G’ (40 °C) (10^3 Pa)	ΔG′	G’ (40 °C) (10^3 Pa)	ΔG′
2% w/w	0.55 ± 0.02 e	1.4	0.35 ± 0.2 d	1.7	0.263 ± 0.004 c	2.2	0.157 ± 0.004 b	2.7	0.101 ± 0.001 a	2.9
4% w/w	3.9 ± 0.3 d	1.4	2.72 ± 0.09 c	1.8	2.0 ± 0.1 b	2.3	1.31 ± 0.03 a	2.6	0.94 ± 0.01 a	2.9
6% w/w	12.6 ± 0.4 d	1.4	9.9 ± 0.9 c	1.7	6.2 ± 0.2 b	2.0	3.9 ± 0.8 a	2.7	2.67 ± 0.03 a	2.9
8% w/w	21.1 ± 0.4 e	1.4	16.1 ± 0.9 d	1.7	12.4 ± 1.6 c	2.1	9.1 ± 0.3 b	2.5	5.3 ± 0.2 a	2.8

ΔG′ = [G′ (4 °C) - G′ (40 °C)]/G′ (40 °C).
Different letters represent significant differences ($p < 0.05$) within rows as derived from ANOVA followed by Duncan post-Hoc test.

the gel network of soy protein. Similarly, Ringgenberg, Alexander, and Corredig (2013) found that GDL-induced gelation of soymilk showed earlier gelation and much stiffer bonds at 7 °C compared to 30 °C, which suggested that hydrogen bonds and van der Waals interactions played a major role in strengthening the network linkages.

Fig. 4C shows that the G′ and G″ of acid-induced gels at 4 °C both increased as the frequency increased from 0.1 to 10 Hz. This indicated the formation of a continuous network and a typical physical gel structure, which normally shows a weak frequency dependence and no crossover of G′ and G″ (Clark & Ross-Murphy, 1987). The frequency dependence of different gels is summarized in Table S1, which showed that the power law exponent of G″, i.e. n″, was slightly higher than the exponent of G′, i.e. n′. Both n′ and n″ of acid-induced gels were not significantly affected by protein concentrations, but gradually increased with the proportion of SPI. Table S2 also shows that the tan δ of gels at 4 °C increased with the proportion of SPI. These results indicated that the LVE properties of gels became less elastically dominated when more WPI was replaced by SPI.

3.5. Non-linear rheology

After the frequency-sweep test, we performed a LAOS strain sweep test on these acid-induced gels to investigate their non-linear viscoelastic (NLVE) properties. Fig. 4D shows all gels displayed a similar strain dependence regardless of the composition and concentration (data for the latter not shown): With increasing intercycle strain amplitude (γ_0), G′ and G″ first displayed a clear plateau, representing the linear viscoelastic (LVE) regime. When γ_0 exceed a certain value, both G′ and G″ decreased gradually, which is known as shear strain softening (Type I) behavior. This non-linear rheological behavior has been explained by a decreased creation rate and increased loss rate of gel network-bonds when γ_0 is increased (Hyun, Kim, Ahn, & Lee, 2002). Similar behavior was also observed for the acid-induced gels formed by pure soy protein (Bi et al., 2017) and peanut protein (Zhu, Li, & Wang, 2019).

The gels displayed similar strain sweep profiles, but the range of their LVE regime, i.e. the critical linear strain (γ_c), significantly changed with protein concentrations and compositions, as shown in Table 2. When the gels were formed at the same protein concentration, γ_c generally

Table 2
Critical linear strain (γ_c) of the acid-induced gels formed at different SPI:WPI ratios.

SPI: WPI	0:4	1:3	2:2	3:1	4:0
Conc.	γ_c [%]	γ_c [%]	γ_c [%]	γ_c [%]	γ_c [%]
2% w/w	42.2 ± 2.2 c	11.3 ± 2.8 b	6.0 ± 0.5 a	5.4 ± 0.4 a	5.6 ± 0.0 a
4% w/w	9.2 ± 0.7 d	8.0 ± 0.2 c	5.5 ± 0.6 b	2.2 ± 0.1 a	2.4 ± 0.1 a
6% w/w	7.9 ± 0.0 d	6.8 ± 0.0 c	5.9 ± 0.3 b	3.2 ± 1.9 a	2.2 ± 0.2 a
8% w/w	6.8 ± 0.5 c	6.4 ± 0.4 c	5.9 ± 0.1 bc	4.8 ± 1.3 b	1.7 ± 0.7 a

Different letters represent significant differences ($p < 0.05$) within rows as derived from ANOVA followed by Duncan post-Hoc test.

decreased as the proportion of SPI increased, indicating that replacing WPI with SPI made the acid-induced gels less ductile. When the gels were formed at the same SPI: WPI ratio, the γ_c dependence on protein concentration was different for the various ratios, which will be further discussed in the next section.

3.5.1. Fractal scaling model

The concentration dependence of G′ and γ_c of protein gels are often given by a power-law relationship, i.e. $G' \sim C^A$, $\gamma_c \sim C^B$, as shown in Fig. S3. Although the G′ (4 °C) of all acid-induced gels increased with protein concentration, the exponent A varied with different SPI: WPI ratios, as shown in Table 3. Pure WPI gels displayed an exponent A of 2.65 which is similar to the results (2.75 ± 0.20) reported by Alting, Hamer, De Kruif, and Visschers (2003). As the proportion of SPI increased, this exponent A gradually increased to 2.96 (for pure SPI gels). The increased exponent A indicated that proteins were used less efficiently in the gelation and distributed more heterogeneously in the structure, which is consistent with the gel morphology observed later on (Fig. 7). For pure WPI and SPI gels, their γ_c decreased with protein concentration, following a power-law model with an exponent B equal to −1.34 and −1.05, respectively. When the gels were formed by WPI and SPI mixtures, the concentration dependence of γ_c became rather different. For the gels formed at SPI: WPI ratio of 1:3, the γ_c decreased with protein concentration, still following a power-law model but with a less negative exponent B (−0.42). For the gels formed at SPI: WPI ratio of 2:2, the γ_c appeared to be independent of the protein concentration. While for the gels formed at SPI: WPI ratio of 3:1, the γ_c first decreased and then increased with protein concentrations (Fig. S3 B).

Shih, Shih, Kim, Liu, and Aksay (1990) has developed a scaling theory for the rheological properties of colloidal gels by considering the gel network as a collection of fractal protein flocs which are closely packed throughout the sample. In their theory, gel structures are classified into a strong-link regime and a weak-link regime. In the strong-link regime, the inter-floc links are stronger than the intra-floc links, and γ_c decreases with increasing protein concentration, while in the weak-link regime, the situation is opposite. Our results indicated that although acid-induced gels formed by pure WPI and SPI could both belong to the strong-link regime, the hybrid gels formed by their mixtures could not be clearly classified as either strong- or weak-link. In these hybrid gels, the interactions and the fractal nature of the flocs seemed to depend on the SPI: WPI ratio. Wu and Morbidelli (2001) further developed Shih's fractal model by introducing a new parameter $\alpha \in [0,1]$ that indicates the relative importance of inter- and intra-floc links in gels. α value of 0 indicates ideal strong-link regime and α value of 1 indicates ideal weak-link regime. With this model an estimate of the fractal dimension (D_f) of the flocs can be obtained based on the concentration dependence of G′ and γ_c: in this extended model $A = [(d-2)+(2+x)(1-\alpha)]/(d-D_f)$, and $B = [1-(2+x)(1-\alpha)]/(d-D_f)$. Here x represents the fractal dimension of the backbone of the flocs (ranging from 1.0 to 1.3 for colloidal gels and assumed to be 1.1 in this study). Table 3 shows that the calculated D_f and α gradually increased for the gels in the order of pure WPI, pure SPI, S:W 1:3 and S:W 2:2. The higher D_f indicated that the constituent flocs had more compact structures. Meanwhile, only for pure WPI gels the α value was close to zero (0.02), indicating only pure WPI gels were of the strong-link type, while other gels that contained SPI were in the intermediate regime.

Table 3
The protein concentration (C) dependence of storage modules (G′) and critical linear strain (γ_c) of the acid-induced gels formed at different SPI:WPI ratios, and the fractal dimension (D_f) calculated based on scaling theory of Wu et al. (2001).

SPI: WPI	$G' \propto C^A$	$\gamma_C \propto C^B$	$A = \frac{(d-2)+(2+x)(1-\alpha)}{d-D_f}$ [a] $B = \frac{1-(2+x)(1-\alpha)}{d-D_f}$		
4 °C	**A**	**B**	D_f	α	
0: 4	2.65	−1.34	1.47	0.02	
1: 3	2.78	−0.42	2.15	0.56	
2: 2	2.84	0.01	2.30	0.68	
3: 1	2.93	–	–	–	
4: 0	2.96	−1.05	1.95	0.32	

[a] The Euclidean dimension d of the gel system is 3 and the backbone fractal dimension x of the flocs is assumed to be 1.1.

3.5.2. Lissajous plots

Since G′ and G″ are based only on the first harmonic contribution to the stress response and may have ambiguous physical meaning in the NLVE regime (Hyun et al., 2011), the intracycle oscillatory response at various intercycle strains (γ_0) or strain rates ($\dot{\gamma}_0$) were analyzed using Lissajous plots. The elastic Lissajous plots (Fig. 5A) and viscous Lissajous plots (Fig. 5B) of 4% w/w gels are constructed by plotting stress (σ) vs. intracycle strain (γ) and stress (σ) vs. intracycle strain rate ($\dot{\gamma}$), respectively. To better illustrate the elastic and viscous contribution to the total stress (σ), the decomposed elastic (σ_e) and viscous stress (σ_v) were also plotted within the loops of the elastic and viscous Lissajous plots, respectively.

As shown in Fig. 5A, at a γ_0 equal to 0.1%, all gels (4% w/w) displayed a narrow and elliptical elastic Lissajous plot, and the σ_e displayed a linear dependence on γ (see straight dashed line). This demonstrated that the deformation amplitude in our SAOS test, i.e. 0.1%, was sufficiently small to ensure all the gels were within the LVE regime. As the γ_0 increased to 10.2%, the shape of the elastic Lissajous plots started to deviate from an elliptic shape due to the impact of higher harmonics presented in the NLVE regime. This distortion was more obvious when the proportion of SPI was higher, which was consistent with our previous results that increasing the SPI: WPI ratio shortened the range of the LVE regime (Table 2). When γ_0 increased to 40.8%, the shapes of the elastic Lissajous plots differed significantly. For the pure WPI gel, the plots were significantly wider than for the other samples and already started to change into a more rhomboidal shape. The area enclosed by the loop and the difference between σ and σ_e both increased significantly, indicating considerable structure breakdown (Schreuders et al., 2021). For hybrid gels formed by WPI and SPI, the loops became progressively narrower with increasing SPI: WPI ratio. The Lissajous plots of these gels displayed a narrow and inverted sigmoidal shape with a steep upswing near maximum γ. The smaller enclosed area of elastic Lissajous plots indicated less dissipated energy per cycle, and the narrower gap between σ and σ_e indicated that the stress response is relatively more elastic dominated. Compared to the relatively straight σ_e curves in the LVE regime, the lower slope of σ_e curves at small intracycle strain [$-0.5 < \gamma < 0.5$] indicates gels have less ability to support elastic stress due to the decreasing number of network bonds, which can be associated with the overall intercycle strain softening observed in Fig. 4D. The steep slope at higher intracycle strain [$\gamma < -0.5$ or $\gamma > 0.5$] could have resulted from the stretching of dissociated flocs, which manifested in an apparent intracycle stiffening (Park, Ahn, & Lee, 2015).

When the γ_0 increased to 128%, the Lissajous plots of pure WPI gels

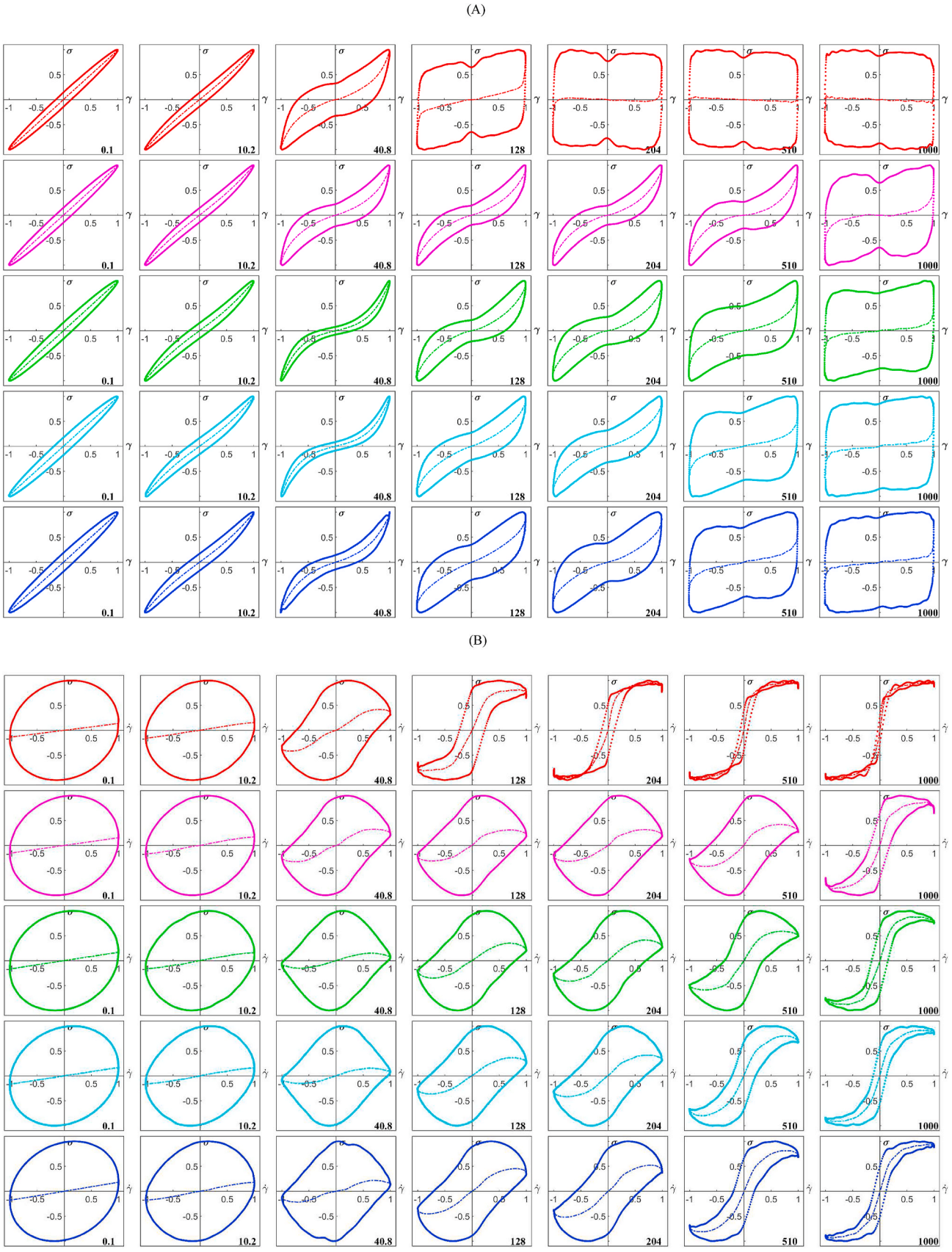

Fig. 5. Elastic Lissajous plots (A) and viscous Lissajous plots (B) of normalized stress (σ/σ_{max}) versus normalized strain (γ/γ_0) or normalized strain rate ($\dot{\gamma}/\dot{\gamma}_0$), for acid-induced gels (4% w/w) formed at different SPI:WPI ratios; S:W 0:4 (red), S:W 1:3 (magenta), S:W 2:2 (green), S:W 3:1 (cyan), S:W 4:0 (dark blue). Solid lines indicate the total stress (σ) and dashed lines within the loop indicates the decomposed elastic stress (σ_e) and viscous stress (σ_v). (For interpretation of the references to color in this figure legend, the reader is referred to the Web version of this article.)

had already changed into a nearly rectangular shape and did not change much further up to the maximum amplitude, i.e. 1000%. This near plastic behavior (Ewoldt, Winter, Maxey, & McKinley, 2010; Schreuders et al., 2021) is evident from an intracycle sequence of (starting from the lower-left corner ($\gamma = -1$) of this curve, in a clockwise direction) elastic straining (the vertical part), yielding, flow (the horizontal part), and recovery. In contrast, this transition to plastic behavior proceeded in a much more gradual way for gels that contained SPI. For pure SPI gels, the Lissajous plots changed into a near rhomboidal shape at $\gamma_0 = 128\%$, and for the hybrid gel formed at SPI: WPI ratio of 1:3, their Lissajous plots had an inverted sigmoidal shape even up to a deformation amplitude of 510%. In addition, while the σ_e of pure WPI gels was near zero for almost the entire cycle when γ_0 reached 204%, one could still observe nonzero values for σ_e when the other gels were subjected to the maximum γ_0 (1020%), a sign there was still residual elasticity in the material. That the gels containing SPI showed a slower transition towards plastic properties and still retained an elastic contribution to the response at higher strain, could be another indication of their coarser network structures, since coarser structures are less prone to a complete transition towards plastic behavior due to increased structural flexibility (Klost, Brzeski, & Drusch, 2020). The higher flexibility could lead to a more gradual decrease in bond numbers, thus some elastic responses can still be detected at higher strain (Klost, Brzeski, & Drusch, 2020).

As a complement to the elastic Lissajous plots, viscous Lissajous plots were shown in Fig. 5B. In contrast to the former, the enclosed area of viscous Lissajous plots represents the stored energy (proportional to G′) per cycle. When γ_0 is 0.1%, all gels displayed circular viscous Lissajous plots, showing that all gels displayed predominantly elastic behavior in the LVE regime. As γ_0 increased, the shape of viscous Lissajous gradually changed into a sigmoidal shape with a decreased enclosed area, which indicated the decay of elasticity. Obviously, this decay started at lower strain rates and proceeded more abruptly in pure WPI gels compared to the other gels. For the gels that contained SPI, a distinct decrease in the stress can be observed near the maximum normalized intracycle strain rate ($\dot{\gamma} = -1$ or 1), which indicated strong intracycle shear thinning behavior. At high deformation amplitude ($\gamma_0 \geq 204\%$), secondary loops were clearly observed in the viscous Lissajous plots of the pure WPI gel, which could be explained by a coupling of the elasticity of sample with instrument inertia (Precha-Atsawanan et al., 2018; Xia et al., 2021).

Overall, we found soy protein plays a dominant role in the non-linear rheological behavior of WPI and SPI hybrid gels, as the evolution of both elastic and viscous Lissajous plots of hybrid gels are more similar to that of pure SPI gels, regardless of the ratios. Even when only 25% WPI was replaced with SPI, the NLVE properties of acid-induced gels changed significantly. This phenomenon can be also found in the gels formed at other concentrations (Fig. S4). Although gels with similar strength (G′) can be obtained by two proteins with different concentrations (e.g. 4% w/w WPI and 6% w/w SPI) (Fig. S3), their NLVE properties still differ a lot (Fig. S5), which demonstrates that the rheological behavior beyond the LVE regime might be a better reflection of the microstructural differences between samples.

3.6. Water holding capacity and gel solubility

Fig. 6A shows the effects of SPI: WPI ratio on the water holding capacity (WHC) of acid-induced gel (4% w/w). The WHC of pure WPI gels was about 88.7%, which was almost three times the WHC of pure SPI gels (33.8%). Increasing the proportion of SPI significantly decreased the WHC of hybrid gels. The WHC of gels has been found closely related to the rheological properties as well as the microstructures of gels. Stiffer gels (with higher G′) generally had larger WHC than less stiff gels, since under the same centrifugal force the stiff gels would experience a lower extent of compression compared to the weaker ones, and hence less water was expelled from the former. This is consistent with our SAOS results. Urbonaite, de Jongh, van der Linden, and Pouvreau (2015) reported that the homogeneity of a gel microstructure significantly

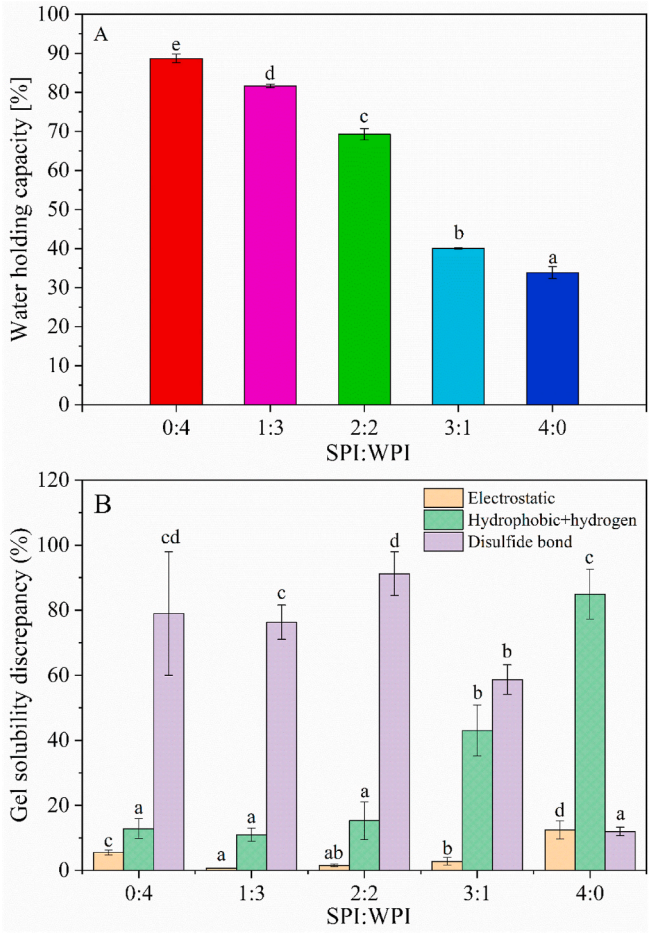

Fig. 6. Water holding capacity and gel solubility of acid-induced gels (4% w/w) formed at different SPI:WPI ratios. Different letters (in the same subplot) indicate the results for different samples have significant differences ($p < 0.05$) according to ANOVA and Duncan post-Hoc test.

contributes to WHC, which is also consistent with the microscopy images of the gel microstructure as shown later (Fig. 7).

Evaluating the gel solubility in the solvents S_A, S_B, S_C, and S_D (see Section 2.7) reveals the types of protein interactions and their relative importance in different gels. As shown in Fig. 6B, both covalent and non-covalent interactions are all involved in the acid-induced gels formed by SPI and WPI, which is consistent with previous studies (Alting, Hamer, De Kruif, Paques, & Visschers, 2003; Rabiey & Britten, 2009). For pure WPI gels, the contribution of disulfide bonds was significantly more important than hydrophobic interactions and hydrogen bonds, and the contribution of electrostatic interactions was the lowest. This is consistent with the study of Alting et al. (2000), who added thiol blocking agents to whey protein aggregate dispersions before acid-induced gelation, and observed a dramatic decrease (5–10-fold) in the gel hardness. Partially replacing WPI with SPI (S:W of 1: 3 or 2: 2) did not change the relative importance of these interactions in the gels, except for the electrostatic interactions which slightly decreased. As SPI became abundant in the gels (S:W > 2:2), the contribution of non-covalent interactions (hydrogen bonds, hydrophobic and electrostatic interactions) significantly increased, while the importance of disulfide bonds significantly decreased, which could be a sign of transition of the dominant gel network as shown later. The increased extent of hydrophobic interactions could be related to the higher surface hydrophobicity of SPI aggregates (Fig. 2E). An increased extent of hydrogen bonding would explain the stronger increase of G′ (higher ΔG′) when these gels were subjected to a cooling step, since hydrogen bonds are

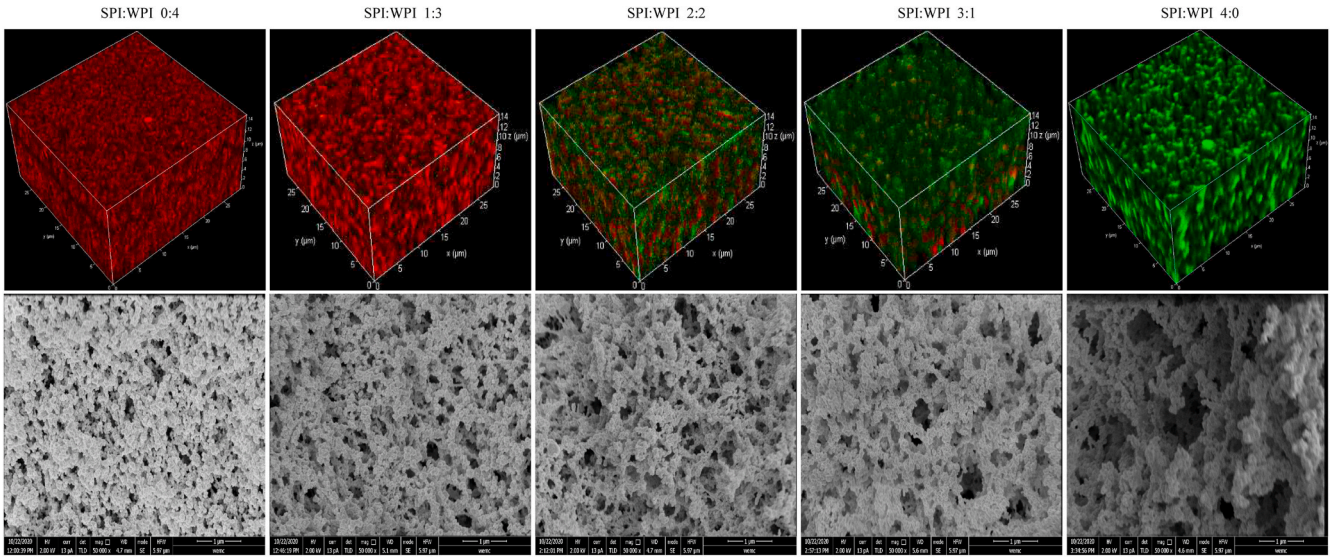

Fig. 7. Multiphoton microscopy (40 × , 3D; WPI dyed in red while SPI in green) (1st row), scanning electron microscopy (50,000 ×) (2nd row) of acid-induced gels formed at different SPI:WPI ratios. (For interpretation of the references to color in this figure legend, the reader is referred to the Web version of this article.)

known to be enhanced at a lower temperature. Although the increased noncovalent interactions are beneficial to the formation of disulfide bonds during acidic gelation (Alting et al., 2000), the much lower composition of sulfur-containing amino acids (Met and Cys) of soy protein compared to whey protein, could substantially limit the formation of disulfide bonds in these SPI-abundant gels (Aoyama et al., 2000).

3.7. Gel morphology

Understanding the relationship between the rheological properties of materials and their microstructures is essential for designing new food products but also a long-term challenge to rheologists. Here, we applied different microscopy techniques to observe the gel microstructure. The first row of Fig. 7 shows 3D images of gel microstructures made using multiphoton laser scanning microscopy (MLSM) with a magnification of 40. Here the SPI and WPI were stained by different dyes and thus are shown in different colors: SPI in green while WPI in red. It can be seen that pure WPI gels showed a denser and more homogenous structure than pure SPI gels. In WPI gels, the constituent flocs appear to be smaller and more evenly distributed in 3D space, while in SPI gels, the flocs were larger and more irregularly shaped, and much larger pores and gaps were observed. Aforementioned results showed that preheated SPI had a lower amount of soluble aggregates and a postponed onset of gelation, which may not be sufficient for a denser and well-arranged network to form. This coarser and looser structure explained why SPI gels showed lower G′, shorter LVE range, and worse WHC than WPI gels, since their less strongly connected and more porous network could be less resilient to deformation, and the water that was originally present in these large gaps and pores could more readily flow out. Replacing WPI with SPI significantly coarsened the gel microstructure, and the gaps and pores increased as the SPI: WPI ratio increased. Similarly, Roesch et al. (2004) also found that the network structures of soy/skim milk mixed GDL-induced gels showed larger pore sizes because of the presence of soy proteins. As mentioned, these coarse networks could explain why gels that contained SPI were less prone to a complete transition towards plastic properties. MLSM also revealed that SPI and WPI appeared to form independent gel networks (Fig. S6). When the SPI: WPI ratio was 1: 3, the network of the hybrid gels was mainly formed by WPI, with SPI embedded as particulate fillers. When the SPI: WPI ratio was 3:1, the situation appeared to be the opposite. When the SPI: WPI ratio was 2: 2, the main network was hard to identify, as the occupancy of each network in 3D space seems to be roughly equal.

The second row of Fig. 7 shows the images obtained by scanning electron microscopy (SEM) with a much higher magnification of 50,000, which provided more detailed information of a cross-section through the gel. SEM shows that all the flocs in the gels consisted of roughly spherical protein particulates. Consistent with the MLSM images, the flocs in pure WPI gel were relatively small and more homogenously distributed. For the gels that contained SPI, the flocs have rougher, more elongated and irregularly branched structures, which appear to be linked to each other by only a few strands, especially obvious when the SPI: WPI ratio was 1: 3 and 2: 2. These results agreed with their higher D_f and α as analyzed by fractal scaling theory. Under deformation, these thin strands could be easily broken, which led to a shorter LVE range. The dissociated flocs would move in the flow field and subsequently be stretched at higher strain, which would explain the apparent intracycle hardening we observed. In addition, since noncovalent interactions played a more important role in samples containing SPI, bonds between flocs could also be more easily reformed. All these features could allow these gels to retain more elasticity even at very high strain, as shown in their Lissajous plots (Fig. 5A). Although the dense, homogeneous, and strong-linked structure allowed WPI gels to resist higher intercycle strain, once the strain exceeds the critical strain, cracks in the microstructure will form more quickly and evenly, leading to a more complete structural breakdown and plastic behavior. These results supported our findings that hybrid gels displayed more similar NLVE properties with pure SPI gels.

4. Conclusions

Acid (GDL)-induced gels with different rheological and microstructural properties can be obtained by mixing commercial SPI and WPI at different ratios and concentrations. Replacing WPI with SPI decreased the stiffness (lower G′) and stretchability (lower γ_c) of acid-induced gels in the linear viscoelastic (LVE) regime, but these hybrid gels displayed a relatively more elastic response in the non-linear viscoelastic (NLVE) regime and a more gradual transition to plastic behavior. The changes in the rheological properties can be correlated to differences in the gel microstructure. Replacing WPI with SPI decreased the proportion of soluble aggregates formed in the preheating step, slowed down the acidification rate of GDL, and postponed the gelling points. As a result, hybrid gels and pure SPI gels displayed coarser and more porous microstructures with lower water holding capacity, compared to pure WPI gels. Replacing WPI with SPI also changed the state of constituent flocs.

The flocs became larger, with rougher, more elongated, and branched structures. The inter-floc links became less strong, and the interactions responsible for gel formation shifted from mainly disulfide bonds to mainly noncovalent interactions. Overall, the results presented here will contribute to the rational design of acid-induced gel foods using whey and soy proteins, since the rheological behavior, especially the one in NLVE regime, is closely related to the sensory attributes of gel-based foods. Further strides could be made to link the current results, especially the LAOS data, with the sensory properties of these gels.

CRediT authorship contribution statement

Wenjie Xia: Conceptualization; Methodology; Investigation; Validation; Formal analysis; Writing-Original Draft; Writing-Review & Editing; Visualization. **Linfeng Zhu:** Investigation; Validation; **Roy J.B. M. Delahaije:** Investigation; Validation; **Zhe Cheng:** Investigation; **Xilong Zhou:** Investigation; **Leonard M.C. Sagis:** Conceptualization; Methodology; Formal analysis; Writing-Review & Editing; Supervision; Project administration; Funding acquisition.

Declaration of competing interest

The authors have declared that no competing interest exists.

Acknowledgements

Author Wenjie Xia appreciates the personal scholarship (No. 201806760056) from China Scholarship Council (CSC), China.

Appendix A. Supplementary data

Supplementary data to this article can be found online at https://doi.org/10.1016/j.foodhyd.2021.107376.

References

Abaee, A., Mohammadian, M., & Jafari, S. M. (2017). Whey and soy protein-based hydrogels and nano-hydrogels as bioactive delivery systems. *Trends in Food Science & Technology, 70*(October), 69–81. https://doi.org/10.1016/j.tifs.2017.10.011

Alting, A. C., Hamer, R. J., De Kruif, C. G., Paques, M., & Visschers, R. W. (2003). Number of thiol groups rather than the size of the aggregates determines the hardness of cold set whey protein gels. *Food Hydrocolloids, 17*(4), 469–479. https://doi.org/10.1016/S0268-005X(03)00023-7

Alting, A. C., Hamer, R. J., De Kruif, C. G., & Visschers, R. W. (2000). Formation of disulfide bonds in acid-induced gels of preheated whey protein isolate. *Journal of Agricultural and Food Chemistry, 48*(10), 5001–5007. https://doi.org/10.1021/jf000474h

Alting, A. C., Hamer, R. J., De Kruif, C. G., & Visschers, R. W. (2003). Cold-set globular protein gels: Interactions, structure and rheology as a function of protein concentration. *Journal of Agricultural and Food Chemistry, 51*(10), 3150–3156. https://doi.org/10.1021/jf0209342

Alting, A. C., Van Der Meulena, E. T., Hugenholtz, J., & Visschers, R. W. (2004). Control of texture of cold-set gels through programmed bacterial acidification. *International Dairy Journal, 14*(4), 323–329. https://doi.org/10.1016/j.idairyj.2003.09.008

Anema, S. G. (2018). Effect of whey protein addition and pH on the acid gelation of heated skim milk. *International Dairy Journal, 79*, 5–14. https://doi.org/10.1016/j.idairyj.2017.11.008

Aoyama, T., Fukui, K., Nakamori, T., Hashimoto, Y., Yamamoto, T., Takamatsu, K., et al. (2000). Effect of soy and milk whey protein isolates and their hydrolysates on weight reduction in genetically obese mice. *Bioscience, Biotechnology and Biochemistry, 64*(12), 2594–2600. https://doi.org/10.1271/bbb.64.2594

Bi, C., Li, D., Wang, L., & Adhikari, B. (2017). Effect of LBG on the gel properties of acid-induced SPI gels. *Lebensmittel-Wissenschaft und -Technologie- Food Science and Technology, 75*, 1–8. https://doi.org/10.1016/j.lwt.2016.08.028

Bi, C., Zhu, Y., Li, L., Zhang, Y., Hua, Z., Zhu, J., et al. (2018). Rheological properties and microstructure of soy protein isolate/κ-carrageenan gels under high-speed shear treatment. *Journal of Food Engineering, 236*, 44–50. https://doi.org/10.1016/j.jfoodeng.2018.05.006

Britten, M., & Giroux, H. J. (2001). Acid-induced gelation of whey protein polymers: Effects of pH and calcium concentration during polymerization. *Food Hydrocolloids, 15*(4–6), 609–617. https://doi.org/10.1016/S0268-005X(01)00049-2

Bryant, C. M., & Julian McClements, D. (1998). Molecular basis of protein functionality with special consideration of cold-set gels derived from heat-denatured whey. *Trends in Food Science & Technology, 9*(4), 143–151. https://doi.org/10.1016/S0924-2244(98)00031-4

Campbell, L. J., Gu, X., Dewar, S. J., & Euston, S. R. (2009). Effects of heat treatment and glucono-δ-lactone-induced acidification on characteristics of soy protein isolate. *Food Hydrocolloids, 23*(2), 344–351. https://doi.org/10.1016/j.foodhyd.2008.03.004

Chihi, M. L., Sok, N., & Saurel, R. (2018). Acid gelation of mixed thermal aggregates of pea globulins and β-lactoglobulin. *Food Hydrocolloids, 85*(March), 120–128. https://doi.org/10.1016/j.foodhyd.2018.07.006

Chu, L., Yang, L., Li, J., Lin, L., & Zheng, G. (2019). Effect of Smilax China L. starch on the gel properties and interactions of calcium sulfate-induced soy protein isolate gel. *International Journal of Biological Macromolecules, 135*, 127–132. https://doi.org/10.1016/j.ijbiomac.2019.05.130

Clark, A. H., & Ross-Murphy, S. B. (1987). Structural and mechanical properties of biopolymer gels. *Biopolymers*. https://doi.org/10.1007/bfb0023332, 57–192.

Day, L. (2013). Proteins from land plants - potential resources for human nutrition and food security. *Trends in Food Science & Technology, 32*(1), 25–42. https://doi.org/10.1016/j.tifs.2013.05.005

Eissa, A. S., & Khan, S. A. (2005). Acid-induced gelation of enzymatically modified, preheated whey proteins. *Journal of Agricultural and Food Chemistry, 53*(12), 5010–5017. https://doi.org/10.1021/jf047957w

Ewoldt, R. H., Hosoi, A. E., & McKinley, G. H. (2008). New measures for characterizing nonlinear viscoelasticity in large amplitude oscillatory shear. *Journal of Rheology, 52*(6), 1427–1458. https://doi.org/10.1122/1.2970095

Ewoldt, R. H., Winter, P., Maxey, J., & McKinley, G. H. (2010). Large amplitude oscillatory shear of pseudoplastic and elastoviscoplastic materials. *Rheologica Acta, 49*(2), 191–212. https://doi.org/10.1007/s00397-009-0403-7

de Faria, J. T., Minim, V. P. R., & Minim, L. A. (2013). Evaluating the effect of protein composition on gelation and viscoelastic characteristics of acid-induced whey protein gels. *Food Hydrocolloids, 32*(1), 64–71. https://doi.org/10.1016/j.foodhyd.2012.12.006

Goudoulas, T. B., & Germann, N. (2017). Phase transition kinetics and rheology of gelatin-alginate mixtures. *Food Hydrocolloids, 66*, 49–60. https://doi.org/10.1016/j.foodhyd.2016.12.018

Gu, X., Campbell, L. J., & Euston, S. R. (2009). Influence of sugars on the characteristics of glucono-δ-lactone-induced soy protein isolate gels. *Food Hydrocolloids, 23*(2), 314–326. https://doi.org/10.1016/j.foodhyd.2008.01.005

Hermansson, A. M. (1986). Soy protein gelation. *Journal of the American Oil Chemists Society, 63*(5), 658–666. https://doi.org/10.1007/BF02638232

Hyun, K., Kim, S. H., Ahn, K. H., & Lee, S. J. (2002). Large amplitude oscillatory shear as a way to classify the complex fluids. *Journal of Non-newtonian Fluid Mechanics, 107*(1–3), 51–65. https://doi.org/10.4103/2319-4170.165000

Hyun, K., Wilhelm, M., Klein, C. O., Cho, K. S., Nam, J. G., Ahn, K. H., et al. (2011). A review of nonlinear oscillatory shear tests: Analysis and application of large amplitude oscillatory shear (Laos). *Progress in Polymer Science, 36*, 1697–1753. https://doi.org/10.1016/j.progpolymsci.2011.02.002

John, J., Ray, D., Aswal, V. K., Deshpande, A. P., & Varughese, S. (2019). Dissipation and strain-stiffening behavior of pectin-Ca gels under Laos. *Soft Matter, 15*(34), 6852–6866. https://doi.org/10.1039/c9sm00709a

Joyner, H. S. (2021). Nonlinear (Large-Amplitude oscillatory shear) rheological properties and their impact on food processing and quality. *Annual Review of Food Science and Technology, 12*, 591–609. https://doi.org/10.1146/annurev-food-061220-100714

Kharlamova, A., Chassenieux, C., & Nicolai, T. (2018). Acid-induced gelation of whey protein aggregates: Kinetics, gel structure and rheological properties. *Food Hydrocolloids, 81*, 263–272. https://doi.org/10.1016/j.foodhyd.2018.02.043

Klost, M., Brzeski, C., & Drusch, S. (2020). Effect of protein aggregation on rheological properties of pea protein gels. *Food Hydrocolloids, 108*(January), Article 106036. https://doi.org/10.1016/j.foodhyd.2020.106036

Klost, M., Giménez-Ribes, G., & Drusch, S. (2020). Enzymatic hydrolysis of pea protein: Interactions and protein fractions involved in fermentation induced gels and their influence on rheological properties. *Food Hydrocolloids, 105*(September 2019). https://doi.org/10.1016/j.foodhyd.2020.105793

Kocher, P. N., & Foegeding, E. A. (1993). Microcentrifuge-based method for measuring water-holding of protein gels. *Journal of Food Science, 58*(5), 1040–1046.

Li, X., Chen, L., Hua, Y., Chen, Y., Kong, X., & Zhang, C. (2020). Effect of preheating-induced denaturation during protein production on the structure and gelling properties of soybean proteins. *Food Hydrocolloids, 105*(October 2019), Article 105846. https://doi.org/10.1016/j.foodhyd.2020.105846

Martin, A. H., De Los Reyes Jiménez, M. L., & Pouvreau, L. (2016). Modulating the aggregation behaviour to restore the mechanical response of acid induced mixed gels of sodium caseinate and soy proteins. *Food Hydrocolloids, 58*, 215–223. https://doi.org/10.1016/j.foodhyd.2016.02.029

Mccann, T. H., Guyon, L., Fischer, P., & Day, L. (2018). Food Hydrocolloids Rheological properties and microstructure of soy-whey protein. *Food Hydrocolloids, 82*, 434–441. https://doi.org/10.1016/j.foodhyd.2018.04.023

Melito, H. S., & Daubert, C. R. (2011). Rheological innovations for characterizing food material properties. *Annual Review of Food Science and Technology, 2*, 153–179. https://doi.org/10.1146/annurev-food-022510-133626

Melito, H. S., Daubert, C. R., & Foegeding, E. A. (2012). Validation of a large amplitude oscillatory shear protocol. *Journal of Food Engineering, 113*(1), 124–135. https://doi.org/10.1016/j.jfoodeng.2012.05.008

Melito, H. S., Daubert, C. R., & Foegeding, E. A. (2013a). Relating large amplitude oscillatory shear and food behavior: Correlation of nonlinear viscoelastic, rheological, sensory and oral processing behavior of whey protein isolate/κ-carrageenan gels. *Journal of Food Process Engineering, 36*(4), 521–534. https://doi.org/10.1111/jfpe.12015

Melito, H. S., Daubert, C. R., & Foegeding, E. A. (2013b). Relationships between nonlinear viscoelastic behavior and rheological, sensory and oral processing behavior of commercial cheese. *Journal of Texture Studies, 44*(4), 253–288. https://doi.org/10.1111/jtxs.12021

Mession, J. L., Roustel, S., & Saurel, R. (2017). Interactions in casein micelle - pea protein system (Part II): Mixture acid gelation with glucono-δ-lactone. *Food Hydrocolloids, 73*, 344–357. https://doi.org/10.1016/j.foodhyd.2017.06.029

Nagano, T., Mori, H., & Nishinari, K. (1994). Rheological properties and conformational states of β-conglycinin gels at acidic pH. *Biopolymers, 34*(2), 293–298. https://doi.org/10.1002/bip.360340215

Nguyen, B. T., Chassenieux, C., Nicolai, T., & Schmitt, C. (2017). Effect of the pH and NaCl on the microstructure and rheology of mixtures of whey protein isolate and casein micelles upon heating. *Food Hydrocolloids, 70*, 114–122. https://doi.org/10.1016/j.foodhyd.2017.03.013

Nicolai, T., Britten, M., & Schmitt, C. (2011). β-Lactoglobulin and WPI aggregates: Formation, structure and applications. *Food Hydrocolloids, 25*(8), 1945–1962. https://doi.org/10.1016/j.foodhyd.2011.02.006

Nicolai, T., & Chassenieux, C. (2019). Heat-induced gelation of plant globulins. *Current Opinion in Food Science, 27*, 18–22. https://doi.org/10.1016/j.cofs.2019.04.005

Nishinari, K., Fang, Y., Guo, S., & Phillips, G. O. (2014). Soy proteins: A review on composition, aggregation and emulsification. *Food Hydrocolloids, 39*, 301–318. https://doi.org/10.1016/j.foodhyd.2014.01.013

Park, J. D., Ahn, K. H., & Lee, S. J. (2015). Structural change and dynamics of colloidal gels under oscillatory shear flow. *Soft Matter, 11*(48), 9262–9272. https://doi.org/10.1039/c5sm01651g

Precha-Atsawanan, S., Uttapap, D., & Sagis, L. M. C. (2018). Linear and nonlinear rheological behavior of native and debranched waxy rice starch gels. *Food Hydrocolloids, 85*(March), 1–9. https://doi.org/10.1016/j.foodhyd.2018.06.050

Rabiey, L., & Britten, M. (2009). Effect of whey protein enzymatic hydrolysis on the rheological properties of acid-induced gels. *Food Hydrocolloids, 23*(8), 2302–2308. https://doi.org/10.1016/j.foodhyd.2009.06.011

Ringgenberg, E., Alexander, M., & Corredig, M. (2013). Effect of concentration and incubation temperature on the acid induced aggregation of soymilk. *Food Hydrocolloids, 30*(1), 463–469. https://doi.org/10.1016/j.foodhyd.2012.05.011

Roesch, R. R., & Corredig, M. (2006). Study of the effect of soy proteins on the acid-induced gelation of casein micelles. *Journal of Agricultural and Food Chemistry, 54*(21), 8236–8243. https://doi.org/10.1021/jf060875i

Roesch, R., Juneja, M., Monagle, C., & Corredig, M. (2004). Aggregation of soy/milk mixes during acidification. *Food Research International, 37*(3), 209–215. https://doi.org/10.1016/j.foodres.2003.11.003

Ryan, K. N., Vardhanabhuti, B., Jaramillo, D. P., van Zanten, J. H., Coupland, J. N., & Foegeding, E. A. (2012). Stability and mechanism of whey protein soluble aggregates thermally treated with salts. *Food Hydrocolloids, 27*(2), 411–420. https://doi.org/10.1016/j.foodhyd.2011.11.006

Schmitt, C., Silva, J. V. C., Amagliani, L., Chassenieux, C., & Nicolai, T. (2019). Heat-induced and acid-induced gelation of dairy/plant protein dispersions and emulsions. *Current Opinion in Food Science, 27*, 43–48. https://doi.org/10.1016/j.cofs.2019.05.002

Schreuders, F. K. G., Sagis, L. M. C., Bodnár, I., Erni, P., Boom, R. M., & van der Goot, A. J. (2021). Small and large oscillatory shear properties of concentrated proteins. *Food Hydrocolloids, 110*(June 2020). https://doi.org/10.1016/j.foodhyd.2020.106172

Shih, W., Shih, W.y., Kim, S., Liu, J., & Aksay, I. A. (1990). Scaling behavior of the elastic properties of colloidal gels. *Physical Review A, 42*(8), 4772–4779.

Spotti, M. J., Loyeau, P. A., Marangón, A., Noir, H., Rubiolo, A. C., & Carrara, C. R. (2019). Influence of Maillard reaction extent on acid induced gels of whey proteins and dextrans. *Food Hydrocolloids, 91*(June 2018), 224–231. https://doi.org/10.1016/j.foodhyd.2019.01.020

Urbonaite, V., de Jongh, H. H. J., van der Linden, E., & Pouvreau, L. (2015). Water holding of soy protein gels is set by coarseness, modulated by calcium binding, rather than gel stiffness. *Food Hydrocolloids, 46*, 103–111. https://doi.org/10.1016/j.foodhyd.2014.12.010

Wang, G., & Guo, M. (2019). Manufacturing technologies of whey protein products. In *Whey protein production, chemistry, functionality, and applications* (pp. 13–37). https://doi.org/10.1002/9781119256052.ch2

Wan, Y., Li, Y., & Guo, S. (2021). Characteristics of soy protein isolate gel induced by glucono-δ-lactone: Effects of the protein concentration during preheating. *Food Hydrocolloids, 113*(June 2020). https://doi.org/10.1016/j.foodhyd.2020.106525

Wu, H., & Morbidelli, M. (2001). Model relating structure of colloidal gels to their elastic properties. *Langmuir, 17*(4), 1030–1036. https://doi.org/10.1021/la001121f

Wu, C., Wang, T., Ren, C., Ma, W., Wu, D., Xu, X., et al. (2020). Advancement of food-derived mixed protein systems: Interactions, aggregations, and functional properties. *Comprehensive Reviews in Food Science and Food Safety*, (October), 1–25. https://doi.org/10.1111/1541-4337.12682

Xia, W., Siu, W. K., & Sagis, L. M. C. (2021). Linear and non-linear rheology of heat-set soy protein gels: Effects of selective proteolysis of β-conglycinin and glycinin. *Food Hydrocolloids, 120*, Article 106962. https://doi.org/10.1016/j.foodhyd.2021.106962

Yang, Z., Hemar, Y., Hilliou, L., Gilbert, E. P., McGillivray, D. J., Williams, M. A. K., et al. (2016). Nonlinear behavior of gelatin networks reveals a hierarchical structure. *Biomacromolecules, 17*(2), 590–600. https://doi.org/10.1021/acs.biomac.5b01538

Zhao, Y. Y., Cao, F. H., Li, X. J., Mu, D. D., Zhong, X. Y., Jiang, S. T., et al. (2020). Effects of different salts on the gelation behaviour and mechanical properties of citric acid-induced tofu. *International Journal of Food Science and Technology, 55*(2), 785–794. https://doi.org/10.1111/ijfs.14348

Zhou, X., Sala, G., & Sagis, L. M. C. (2020). Bulk and interfacial properties of milk fat emulsions stabilized by whey protein isolate and whey protein aggregates. *Food Hydrocolloids*. , Article 106100. https://doi.org/10.1016/j.foodhyd.2020.106100

Zhu, Y. dan, Li, D., & Wang, L. jun (2019). Dynamic rheological properties of peanut protein isolate and aggregation suspension and acid-induced gel. *Powder Technology, 358*, 95–102. https://doi.org/10.1016/j.powtec.2018.08.052